

Article

LPE Growth of Single Crystalline Film Scintillators Based on Ce^{3+} Doped $\text{Tb}_{3-x}\text{Gd}_x\text{Al}_{5-y}\text{Ga}_y\text{O}_{12}$ Mixed Garnets

Vitalii Gorbenko ^{1,*}, Tetiana Zorenko ¹, Sandra Witkiewicz ¹, Kazimierz Paprocki ¹, Oleg Sidletskiy ², Alexander Fedorov ³, Paweł Bilski ⁴ , Anna Twardak ⁴ and Yuriy Zorenko ^{1,*} 

¹ Institute of Physics, Kazimierz Wielki University in Bydgoszcz, 85090 Bydgoszcz, Poland; tzorenko@ukw.edu.pl (T.Z.); s-witkiewicz@wp.pl (S.W.); paprocki@ukw.edu.pl (K.P.)

² Institute for Scintillation Materials, National Academy of Sciences of Ukraine, 61001 Kharkiv, Ukraine; osidletskiy@yahoo.com

³ SSI Institute for Single Crystals, National Academy of Sciences of Ukraine, 61178 Kharkiv, Ukraine; fedorov@xray.isc.kharkov.com

⁴ Institute of Nuclear Physics, Polish Academy of Sciences, 31342 Krakow, Poland; pawel.bilski@ifj.edu.pl (P.B.); anna.twardak@gmail.com (A.T.)

* Correspondence: gorbenko@ukw.edu.pl (V.G.); zorenko@ukw.edu.pl (Y.Z.)

Received: 24 July 2017; Accepted: 25 August 2017; Published: 30 August 2017

Abstract: The growth of single crystalline films (SCFs) with excellent scintillation properties based on the $\text{Tb}_{1.5}\text{Gd}_{1.5}\text{Al}_{5-y}\text{Ga}_y\text{O}_{12}:\text{Ce}$ mixed garnet at $y = 2\text{--}3.85$ by Liquid Phase Epitaxy (LPE) method onto $\text{Gd}_3\text{Al}_{2.5}\text{Ga}_{2.5}\text{O}_{12}$ (GAGG) substrates from BaO based flux is reported in this work. We have found that the best scintillation properties are shown by $\text{Tb}_{1.5}\text{Gd}_{1.5}\text{Al}_3\text{Ga}_2\text{O}_{12}:\text{Ce}$ SCFs. These SCFs possess the highest light yield (LY) ever obtained in our group for LPE grown garnet SCF scintillators exceeding by at least 10% the LY of previously reported $\text{Lu}_{1.5}\text{Gd}_{1.5}\text{Al}_{2.75}\text{Ga}_{2.25}\text{O}_{12}:\text{Ce}$ and $\text{Gd}_3\text{Al}_{2-2.75}\text{Ga}_{3-2.25}\text{O}_{12}:\text{Ce}$ SCF scintillators, grown from BaO based flux. Under α -particles excitation, the $\text{Tb}_{1.5}\text{Gd}_{1.5}\text{Al}_3\text{Ga}_2\text{O}_{12}:\text{Ce}$ SCF show LY comparable with that of high-quality $\text{Gd}_3\text{Al}_{2.5}\text{Ga}_{2.5}\text{O}_{12}:\text{Ce}$ single crystal (SC) scintillator with the LY above 10,000 photons/MeV but faster (at least by 2 times) scintillation decay times $t_{1/e}$ and $t_{1/20}$ of 230 and 730 ns, respectively. The LY of $\text{Tb}_{1.5}\text{Gd}_{1.5}\text{Al}_{2.5}\text{Ga}_{2.5}\text{O}_{12}:\text{Ce}$ SCFs, grown from PbO flux, is comparable with the LY of their counterparts grown from BaO flux, but these SCFs possess slightly slower scintillation response with decay times $t_{1/e}$ and $t_{1/20}$ of 330 and 990 ns, respectively. Taking into account that the SCFs of the $\text{Tb}_{1.5}\text{Gd}_{1.5}\text{Al}_{3-2.25}\text{Ga}_{2-2.75}\text{O}_{12}:\text{Ce}$ garnet can also be grown onto Ce^{3+} doped GAGG substrates, the LPE method can also be used for the creation of the hybrid film-substrate scintillators for simultaneous registration of the different components of ionization fluxes.

Keywords: liquid phase epitaxy; single crystalline films; scintillators; mixed garnets; Tb^{3+} cations

1. Introduction

The development of detectors for 2D/3D microimaging using X-ray sources and synchrotron radiation demands the creation of thin (from a few microns thick up to 20 microns) single crystalline film (SCF) scintillating screens with an extremely high ability for X-ray absorption and a micron-submicron spatial resolution [1–4]. More recently, for this purpose, the visible emitting scintillating screens based on the SCF of Ce doped $\text{Y}_3\text{Al}_5\text{O}_{12}$ (YAG) and $\text{Lu}_3\text{Al}_5\text{O}_{12}$ (LuAG) garnets grown by the Liquid Phase Epitaxy (LPE) method have been used and the spatial resolution of the detector in the micron range has been achieved using synchrotron radiation with energy in the 8–20 keV range [1,2]. After that, the SCFs of Eu^{3+} , Tb^{3+} doped $\text{Gd}_3\text{Al}_5\text{O}_{12}$ (GGG) and Sc^{3+} doped LuAG garnets [3,4], Tb^{3+} and double Tb^{3+} , Ce^{3+} doped Lu_2SiO_5 (LSO) orthosilicates [5–14], Ce^{3+} , Tb^{3+} and

Eu^{3+} doped LuAlO_3 (LuAP) and $(\text{Gd,Lu})\text{AlO}_3$ (GLAP) perovskites [15–19] and recently Ce^{3+} doped $\text{Tb}_3\text{Al}_5\text{O}_{12}$ (TbAG) garnets [20,21], have also been successfully developed in the last decade for microimaging detectors using the LPE method.

The fabrication of screens with higher spatial resolution of X-ray images in the submicron range demands the creation of new scintillating film screens with extremely high absorption ability for X-rays—which is proportional to ρZ_{eff}^4 , where ρ is the density and Z_{eff} is the effective atomic number of scintillators [2,3]—as well as the development of novel concepts for microimaging.

During the last years, two novel concepts for the creation of a detector for microtomography have been proposed [15,19,21]. The first concept is related to the engineering of K-edge of X-ray absorption multilayer-film scintillators using the solid solution of oxide compounds containing the Lu, Gd and Tb ions [15,19,21]. Indeed, the absorption ability of the film scintillator can be significantly improved in the 20–65 keV range due to the significant broadening of the K-edge of X-ray absorption in such mixed materials [15,19,21]. The second concept is based on using the complex multilayer-film scintillator with a separate pathway for registration of the optical signal from each layer and final overlapping of the images coming from the different parts of the complex scintillator [15,21]. By using such multilayer-film scintillators one can significantly improve the contrast and resolution of images even in the submicron range. Two such novel concepts also demand the fabrication of different sets of heavy and efficient SCF scintillators which can be deposited onto the same substrates.

The Ce^{3+} doped $\text{Lu}_{3-x}\text{Gd}_x\text{Al}_{5-y}\text{Ga}_y\text{O}_{12}$ and $\text{Gd}_3\text{Al}_{5-y}\text{Ga}_y\text{O}_{12}$ mixed garnets are related to the efficient and heavy scintillators with very high (up to 50,000 photons/MeV) light yield (LY) under γ quanta excitation [22–25]. For this reason, these compounds are also used for the fabrication of the scintillation screens with high absorption ability for X-rays [26–33]. With the aim of increasing the energy transfer efficiency from the host of mixed garnets to the Ce^{3+} ions, the $\text{Tb}_3\text{Al}_5\text{O}_{12}$, $\text{Lu}_{3-x}\text{Tb}_x\text{Al}_5\text{O}_{12}$ and $\text{Gd}_{3-x}\text{Tb}_x\text{Al}_5\text{O}_{12}$ SCFs were also crystallized by the LPE method and their luminescent and scintillation properties were investigated [20,21,34,35]. The Ga co-doped analogues of these garnets can also be considered as very interesting matrixes for this purpose and their luminescent and scintillation properties were briefly reported by us as well [36]. At the same time, the possibility of the creation of the efficient SCF scintillators on the basis of the mentioned Tb containing garnets by the LPE method still needs the following technological and experimental evidence. First of all, estimation of the real potential of different garnet compositions for producing the scintillation screens strongly requires the LPE crystallization of these compounds in the SCF form from the different types of fluxes due to very large influence of flux related dopants on their scintillation characteristics [31,33,37,38] as well as the crystal analogs of these garnets using MPD [39] or Czochralski methods.

In this paper, we present the new results of the research on the creation of the advanced SCF scintillation screens based on Ce doped $\text{Tb}_{1.5}\text{Gd}_{1.5}\text{Al}_{5-y}\text{Ga}_y\text{O}_{12}$ mixed garnets at $y = 2\text{--}3.85$, grown by the LPE method from the novel lead free BaO based flux (later called $\text{Tb}_{1.5}\text{Gd}_{1.5}\text{Al}_{5-y}\text{Ga}_y\text{O}_{12}:\text{Ce}$ (BaO) SCFs) and compare their properties with those of $\text{Tb}_{3-x}\text{Gd}_x\text{Al}_{5-y}\text{Ga}_y\text{O}_{12}$ SCFs at $x = 0\text{--}2.1$ and $y = 0\text{--}2.75$, grown from the traditional PbO based flux [21,37] (later called $\text{Tb}_{3-x}\text{Gd}_x\text{Al}_{5-y}\text{Ga}_y\text{O}_{12}:\text{Ce}$ (PbO) SCFs).

For engineering the scintillator composition we apply the combination of Ce^{3+} 5d-level positioning [20] and band-gap engineering [40] in the Ce doped $\text{Tb}_{3-x}\text{Gd}_x\text{Al}_{5-y}\text{Ga}_y\text{O}_{12}$ mixed garnet using the substitution by Gd^{3+} cations of the dodecahedral sites of $\text{Tb}_3\text{Al}_5\text{O}_{15}$ garnet lattice with the concentration $x = 1.5$ and the substitution by Ga^{3+} ions of the Al^{3+} cations in both the tetrahedral and octahedral positions of the garnet host at concentration $y = 2\text{--}3.85$. Additionally, we can expect an increase in the energy transfer efficiency from the host of the $\text{Tb}_{3-x}\text{Gd}_x\text{Al}_{5-y}\text{Ga}_y\text{O}_{12}$ garnet to the Ce^{3+} ions using the sublattices of Tb^{3+} and Gd^{3+} cations.

2. Growth of $\text{Tb}_{3-x}\text{Gd}_x\text{Al}_{5-y}\text{Ga}_y\text{O}_{12}:\text{Ce}$ Single Crystalline Films

The SCFs of $\text{Tb}_{3-x}\text{Gd}_x\text{Al}_{5-y}\text{Ga}_y\text{O}_{12}:\text{Ce}$ garnets were grown by the LPE method onto $\text{Gd}_3\text{Al}_2.5\text{Ga}_{2.5}\text{O}_{12}$ (GAGG) substrates with a relatively high lattice constant of 12.228 Å in comparison with

the traditional $\text{Y}_3\text{Al}_5\text{O}_{12}$ (YAG) substrates with a lattice constant of 12.003 Å from supercooled melt solutions using both $\text{BaO-B}_2\text{O}_3\text{-BaF}_2$ and $\text{PbO-B}_2\text{O}_3$ fluxes. Firstly, the sets of optical quality perfect SCF samples—with x values in the 0–2.1 range, y values changing in the 0–2.85 range and thickness in the 16–38 μm range—were crystallized onto GAGG substrates with a square of $1 \times 1 \text{ cm}^2$ with the (100) orientation (Figure 1, left) using the conventional PbO flux for more detail determination of the optimal ranges of Gd and Ga concentrations x and y , respectively, in comparison with work [36]. After that, other sets of optically good quality $\text{Tb}_{1.5}\text{Gd}_{1.5}\text{Al}_{5-y}\text{Ga}_y\text{O}_{12}:\text{Ce}$ SCF samples—with y values changing in the 2–3.8 range and thickness in the 10.5–22 μm range—were also successfully crystallized onto GAGG substrates from novel lead-free BaO based flux (see Figure 1, middle and right figures, and Table 1). The components of this flux have significantly smaller influence on their scintillation properties than in the case of PbO flux grown SCF scintillators [31,33,37,38]. At the same time, the high viscosity of this BaO based flux leads to formation of different structural macro-defects and strongly decreases the uniformity of SCF surface [31,33,37]. Such unwanted effects are also observed in the case of growing the $\text{Tb}_{1.5}\text{Gd}_{1.5}\text{Al}_{5-y}\text{Ga}_y\text{O}_{12}:\text{Ce}$ SCFs from BaO based flux. For this reason, *using the PbO-B₂O₃ solvent—due to its low viscosity and good kinematic properties—is preferable for producing high quality SCF scintillators* for ensuring the best structural and surface quality of screens for high-resolution X-ray imaging [6,7,18,19].



Figure 1. Images of undoped $\text{Gd}_3\text{Al}_2.5\text{Ga}_{2.5}\text{O}_{12}$ (GAGG) substrate (left), $\text{Tb}_3\text{Al}_2.5\text{Ga}_{2.5}\text{O}_{12}:\text{Ce}$ (PbO) (middle) and $\text{Tb}_{1.5}\text{Gd}_{1.5}\text{Al}_3\text{Ga}_2\text{O}_{12}:\text{Ce}$ (BaO) (right) SCF scintillators, grown by the LPE method onto GAGG substrates.

Table 1. Growth conditions, luminescent and scintillation properties of $\text{Tb}_{3-x}\text{Gd}_x\text{Al}_{5-y}\text{Ga}_y\text{O}_{12}:\text{Ce}$ SCFs. M—SCF/substrate misfit, λ_{max} —maximum of CL spectra, $t_{1/e}$ and $t_{1/20}$ scintillation decay times to 1/e and 1/20 levels, respectively; LY—photoelectron light yield under α -particle excitation by ^{239}Pu (5.15 MeV) source with respect to the standard YAG:Ce SCF with a photoelectron LY of 360 phels/MeV (light yield of 2650 photons/MeV) [38] and reference $\text{Gd}_3\text{Al}_{2-2.5}\text{Ga}_{3-2.5}\text{O}_{12}:\text{Ce}$ bulk crystals with a photoelectron LY of 1300–1370 phels/MeV (light yield of about 10,100 photons/MeV).

Content of SCF Samples	Flux	Substrate	m, %	λ_{max} , nm	$t_{1/e}/t_{1/20}$, ns	LY, %	Reference
YAG:Ce	PbO	YAG	-	535	67.3	100	[21,31]
LuAG:Ce	PbO	YAG	-0.82	509	52.8	205	[21,31]
$\text{Tb}_{1.5}\text{Gd}_{1.5}\text{Al}_3\text{Ga}_2\text{O}_{12}:\text{Ce}$	BaO	GAGG	-1.30	553	228/728	380	
$\text{Tb}_{1.5}\text{Gd}_{1.5}\text{Al}_{2.5}\text{Ga}_{2.5}\text{O}_{12}:\text{Ce}$	BaO	GAGG	-0.79	543	201/893	270	
$\text{Tb}_{1.5}\text{Gd}_{1.5}\text{Al}_{1.5}\text{Ga}_{3.5}\text{O}_{12}:\text{Ce}$	BaO	GAGG	+0.05	543	183/728	160	
$\text{Tb}_{1.5}\text{Gd}_{1.5}\text{Al}_{1.15}\text{Ga}_{3.85}\text{O}_{12}:\text{Ce}$	BaO	GAGG	+0.5	543	103/868	50	
$\text{Tb}_3\text{Al}_5\text{O}_{12}:\text{Ce}$	PbO	GAGG	-1.29	560	306/1795	195	[21]
$\text{Tb}_3\text{Al}_3\text{Ga}_2\text{O}_{12}:\text{Ce}$	PbO	GAGG	-0.49	543	435/1340	200	[36]
$\text{Tb}_3\text{Al}_{2.5}\text{Ga}_{2.5}\text{O}_{12}:\text{Ce}$	PbO	GAGG	-0.37	543	456/1368	235	[36]
$\text{Tb}_2\text{GdAl}_{2.5}\text{Ga}_{2.5}\text{O}_{12}:\text{Ce}$	PbO	GAGG	-0.20	543	291/883	254	[36]
$\text{Tb}_{1.5}\text{Gd}_{1.5}\text{Al}_{2.5}\text{Ga}_{2.5}\text{O}_{12}:\text{Ce}$	PbO	GAGG	-0.12	543	333/990	380	[36]
$\text{TbGd}_2\text{Al}_{2.5}\text{Ga}_{2.5}\text{O}_{12}:\text{Ce}$	PbO	GAGG	-0.04	543	299/88	160	[36]
$\text{Gd}_3\text{Al}_{2.5}\text{Ga}_{2.5}\text{O}_{12}:\text{Ce}$ SC	-	-	-	547	441/1536	381	[21,31]
$\text{Gd}_3\text{Al}_2\text{Ga}_3\text{O}_{12}:\text{Ce}$ SC	-	-	-	549	240/876	365	[21,31]

The concentration of CeO_2 activating oxide was 10 and 5 mole% with respect to the garnet-forming components in the cases of SCF growth using PbO and BaO based fluxes, respectively.

The composition of SCF samples was determined using a JEOL JSM-820 electronic microscope, equipped by an EDX microanalyzer with IXRF 500 and LN2 Eumex detectors. From the microanalysis of the content of the SCF samples we have also found that the segregation coefficient of Ga^{3+} ions in $Tb_3Al_{5-y}Ga_yO_{12}:Ce$ and $Tb_{3-x}Gd_xAl_{5-y}Ga_yO_{12}:Ce$ SCFs, grown from PbO based flux, was equal to 0.59–0.65 and 0.735–0.82, respectively (Table 2). The segregation coefficient of Gd^{3+} ions in $Tb_{3-x}Gd_xAl_{5-y}Ga_yO_{12}:Ce$ (PbO) SCFs was equal to 0.95–1.05. The segregation coefficient of Ce^{3+} ions was equal to about 0.004–0.005 and 0.0095–0.02 in $Tb_3Al_{5-y}Ga_yO_{12}:Ce$ SCF and $Tb_{3-x}Gd_xAl_{5-y}Ga_yO_{12}:Ce$ SCFs, in the case of using PbO based flux for their growth (Table 2).

We have also found that the segregation coefficients of Ga^{3+} and Ce^{3+} ions in $Tb_{3-x}Gd_xAl_{5-y}Ga_yO_{12}:Ce$ SCFs in the case of using BaO based flux were significantly larger. Specifically, the segregation coefficient of Ga^{3+} ions in these SCFs, grown from BaO based flux, was equal to 1.0–1.1 and was notably larger than the respective values in the SCFs grown from PbO based flux (Table 2). The segregation coefficient of Ce^{3+} ions in the $Tb_{3-x}Gd_xAl_{5-y}Ga_yO_{12}:Ce$ SCFs was also significantly larger in the case of using BaO based flux and was equal to 0.012–0.14 in comparison with the 0.004–0.005 value in $Tb_3Al_{5-y}Ga_yO_{12}:Ce$ and 0.0095–0.02 in $Tb_{3-x}Gd_xAl_{5-y}Ga_yO_{12}:Ce$ SCF counterparts grown from PbO based flux (Table 2). At the same time, the segregation coefficient of Gd^{3+} ions, being equal to 1.0–1.1 in the case of $Tb_{3-x}Gd_xAl_{5-y}Ga_yO_{12}:Ce$ SCFs, grown from BaO based flux, was only slightly larger than that in the case of using PbO based flux (Table 2).

The XRD measurements (spectrometer DRON 4, $Cu_{K\alpha}$ X-ray source) were used for characterization of the structural quality of $Tb_{1.5}Gd_{1.5}Al_{5-y}Ga_yO_{12}:Ce$ SCFs, grown from BaO based flux (Figure 2). From the respective XRD patterns of these SCFs at y value in the 2–3.85 range (Figure 2), we can also estimate the lattice constants of the different garnet compositions and the misfit between the lattice constants of SCFs and GAGG substrate $\Delta a = (a_{SCF} - a_{sub})/a_{sub} \times 100\%$ (Table 1). Namely, the lattice constant of $Tb_{1.5}Gd_{1.5}Al_{5-y}Ga_yO_{12}:Ce$ (BaO) SCFs at $y = 2-3.85$ changed from 12.069 Å for $Tb_{1.5}Gd_{1.5}Al_3Ga_2O_{12}:Ce$ SCFs to 12.2913 Å for $Tb_{1.5}Gd_{1.5}Al_{1.2}Ga_{3.8}O_{12}:Ce$ SCFs (Figure 2) and the value of misfit m changed from -1.3% to $+0.52\%$ for these SCF samples (Table 1).

Table 2. Segregation coefficients of different ions in $Tb_{3-x}Gd_xAl_{5-y}Ga_yO_{12}:Ce$ SCFs grown onto GAGG substrates.

Garnet Content	Type of Flux	Segregation Coefficient		
		Gd^{3+}	Ga^{3+}	Ce^{3+}
$Tb_3Al_{5-2.9}Ga_{0-2.1}O_{12}:Ce$	PbO		0.59–0.65	0.004–0.005
$Tb_{2-0.9}Gd_{1-2.1}Al_{2.25-2.4}Ga_{2.75-2.6}O_{12}:Ce$	PbO	1.0–1.1	0.735–0.82	0.0095–0.02
$Tb_{1.5}Gd_{1.5}Al_{3-1.15}Ga_{2-3.85}O_{12}:Ce$	BaO	1.0–1.05	1.0–1.1	0.012–0.14

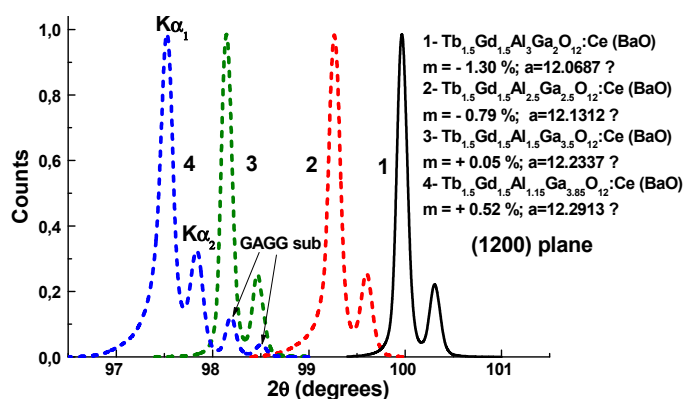


Figure 2. XRD patterns of (1200) planes of $Tb_{1.5}Gd_{1.5}Al_{5-y}Ga_yO_{12}:Ce$ (BaO) SCFs at $y = 2$ (1); 2.5 (2); 3.5 (3) and 3.85 (4). The film/substrate lattice misfit m lies in the $-1.3\% < m < +0.5\%$ range.

The measurements of rocking curves in the ω and 2θ - ω scanning modes were applied for characterization of the structural quality of $\text{Tb}_{1.5}\text{Gd}_{1.5}\text{Al}_{5-y}\text{Ga}_y\text{O}_{12}:\text{Ce}$ (BaO) SCFs at different Ga content y in the 2.0–3.85 range (Figure 3a,b, respectively). As can be seen from these figures, the quality of the SCFs, which is proportional to FWHM of rocking curves, significantly increases at lower SCF-substrate misfit values m in $\text{Tb}_{1.5}\text{Gd}_{1.5}\text{Al}_{5-y}\text{Ga}_y\text{O}_{12}:\text{Ce}$ (BaO) SCFs. Namely, the smallest FWHM values of 0.0182 and 0.0121 degrees are observed for $\text{Tb}_{1.5}\text{Gd}_{1.5}\text{Al}_{1.5}\text{Ga}_{3.5}\text{O}_{12}:\text{Ce}$ (BaO) SCFs (Figure 3a,b, respectively) grown onto GAGG substrates with the lowest SCF/substrate misfit value $m = +0.05\%$ (Table 1).

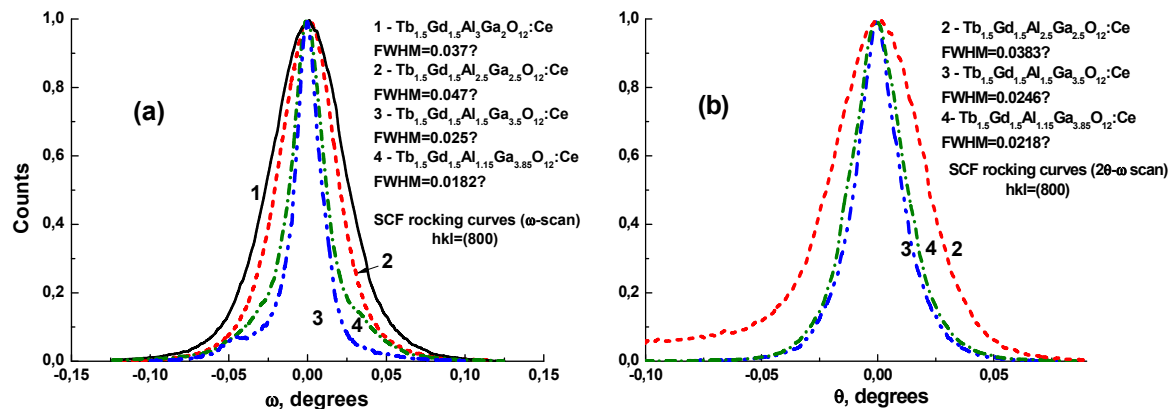


Figure 3. Rocking curves of $\text{Tb}_{1.5}\text{Gd}_{1.5}\text{Al}_{5-y}\text{Ga}_y\text{O}_{12}:\text{Ce}$ (BaO) SCFs grown onto GGAG substrates at different y values: $y = 2$ (1); 2.5 (2); 3.5 (3) and 3.85 (4) recorded in ω (a) and 2θ - ω (b) scanning modes.

3. Luminescent and Scintillation Properties of $\text{Tb}_{3-x}\text{Gd}_x\text{Al}_{5-y}\text{Ga}_y\text{O}_{12}:\text{Ce}$ Single Crystalline Films

For characterization of the optical properties of Ce^{3+} doped $\text{Tb}_{3-x}\text{Gd}_x\text{Al}_{5-y}\text{Ga}_y\text{O}_{12}:\text{Ce}$ SCFs, the cathodoluminescence (CL) spectra, LY and scintillation decay kinetics measurements as well as the thermostimulated luminescence (TSL) glow curves under excitation by α -particles were performed.

The CL spectra were measured at the room temperature (RT) using an electron microscope SEM JEOL JSM-820, additionally equipped with a spectrometer Stellar Net with TE-cooled CCD detector working in the 200–1200 nm range. The scintillation LY with a shaping time of 14 μs and decay kinetics measurements were performed using the setup based on a Hamamatsu H6521 PMT, multichannel analyzer and digital TDS3052 oscilloscope under excitation by α -particles of Pu^{239} (5.15 MeV) source. The energy resolution (ER) of SCF scintillators is calculated as a ratio of the FWHM of the full energy peak to the peak's centroid position: $E = \text{FWHM}/\text{centroid} [\%]$. The TSL measurements were performed in the 300–800 K temperature range using a commercial Risoe DA-20 TL/OSL reader (Denmark) after α -particle excitation by the Am^{241} source which is built into the DA-20 reader. The TL glow curves were registered from 50 $^\circ\text{C}$ to 450 $^\circ\text{C}$ at the rate of 5 $^\circ\text{C}\cdot\text{s}^{-1}$. The measurements were conducted with a Shott BG 39 green filter, with transmission from 350 to 700 nm. This filter is well adapted for the registration of Ce^{3+} luminescence in the SCF samples under study. Meanwhile, the spectrally resolved TSL spectra of $\text{Tb}_{3-x}\text{Gd}_x\text{Al}_{5-y}\text{Ga}_y\text{O}_{12}$ SCF with different Gd^{3+} and Tb^{3+} content (not present in the paper) show only Ce^{3+} luminescence in the green-yellow ranges and absence of the emission of Tb^{3+} or Gd^{3+} cations.

3.1. Cathodoluminescence Spectra

The RT CL spectra of $\text{Tb}_3\text{Al}_{5-y}\text{Ga}_y\text{O}_{12}:\text{Ce}$ and $\text{Tb}_{3-x}\text{Gd}_x\text{Al}_{5-y}\text{Ga}_y\text{O}_{12}:\text{Ce}$ SCFs, grown from PbO based flux, with close y values in the 2–2.5 range and different x values in the 0–2 range, are shown in Figure 4a,b, respectively, in comparison with the spectrum of TbAG:Ce SCF (Figure 4a, curve 1). The RT CL spectra of $\text{Tb}_{1.5}\text{Gd}_{1.5}\text{Al}_{5-y}\text{Ga}_y\text{O}_{12}:\text{Ce}$ SCFs, grown from BaO based flux, with different y

values in the 2–3.85 range, are presented in Figure 4c, curves 1–4 in comparison with the CL spectra of standard $Gd_3Al_{2.5}Ga_{2.5}O_{12}:Ce$ bulk SC (Figure 4b, curve 5).

The CL spectra of all the SCFs under study show only the dominant luminescence of Ce^{3+} or Tb^{3+} ions in the visible range without any bands in the UV range related to the luminescence of antisite defects [41–44], which typically are observed in the bulk crystal analogues of these garnets [45,46].

The results, presented in Figure 4a–c, indicate that the complicated $Gd^{3+} \rightarrow Tb^{3+} \rightarrow Ce^{3+} \rightarrow Tb^{3+}$ cascade energy transfer is observed in the $Tb_{3-x}Gd_xAl_{5-y}Ga_yO_{12}:Ce$ mixed garnet, with large content of Gd^{3+} and Ga^{3+} cations due to overlapping of the Gd^{3+} and Tb^{3+} emission bands and the absorption bands of Tb^{3+} and Ce^{3+} ions [47–51]. Namely, the change of the positions of Ce^{3+} and Tb^{3+} 4f–5d absorption and emission bands at different concentrations of Tb^{3+} , Gd^{3+} and Ga^{3+} cations leads to a strong variation of the efficiency of $Gd^{3+} \rightarrow Tb^{3+} \rightarrow Ce^{3+} \rightarrow Tb^{3+}$ energy transfer processes in $Tb_{3-x}Gd_xAl_{5-y}Ga_yO_{12}:Ce$ SCFs and results in the respective changes of their CL spectra (Figure 4a–c).

The estimation of the optimal content of Gd^{3+} and Ga^{3+} cations in $Tb_{3-x}Gd_xAl_{5-y}Ga_yO_{12}:Ce$ SCFs in the $x = 1–1.5$ and $y = 2–3$ ranges was firstly performed in [36]. We will explain such a choice in this work in more detail based on the results of their CL spectra (Figure 4a,b). Alloying of Ga^{3+} ions in $Tb_3Al_5O_{12}:Ce$ (PbO) SCF in the concentration range above $x = 2$ leads to a decrease of the garnet band gap value [34] and increasing the centroid shift of O–Ga bonding in comparison with O–Al bonding. That results in the subsequent blue shift of the Ce^{3+} emission spectra in $Tb_3Al_{5-y}Ga_yO_{12}:Ce$ (PbO) SCFs (Figure 4a, curves 2 and 3) and $Tb_{1.5}Gd_{1.5}Al_{5-y}Ga_yO_{12}:Ce$ (BaO) SCFs (Figure 4c, curves 1–4). It is most important here that increasing the level of Ga^{3+} alloying in these SCFs above $y = 2–2.5$ also leads to a strong decrease of the Ce^{3+} emission contribution to the total spectrum of the CL luminescence of these SCF samples (Figure 4a,c).

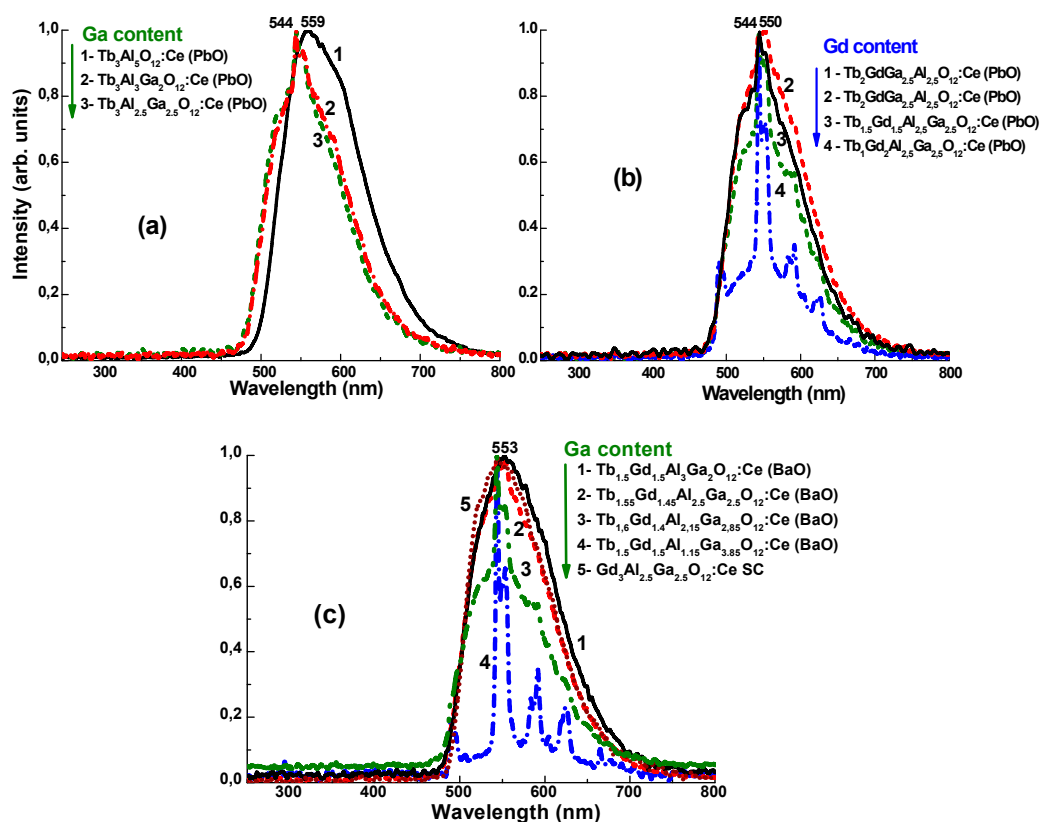


Figure 4. Normalized CL spectra at 300 K of $Tb_3Al_{5-y}Ga_yO_{12}:Ce$ (PbO) (a), $Tb_{3-x}Gd_xAl_{5-y}Ga_yO_{12}:Ce$ (PbO) (b) and $Tb_{3-x}Gd_xAl_{5-y}Ga_yO_{12}:Ce$ (BaO) (c) SCFs with different x and y values (see legend of the figure) in comparison with CL spectra of $Tb_3Al_5O_{12}:Ce$ (PbO) SCF (1a) and $Gd_3Al_{2.5}Ga_{2.5}O_{12}:Ce$ bulk SC (5b).

Alloying of Gd^{3+} ions in $Tb_3Al_{5-y}Ga_yO_{12}:Ce$ (PbO) SCFs in the concentration range $x = 0-1.5$ has an opposite effect than the Ga^{3+} alloying and leads to the notable red shift of their CL spectra. The Gd^{3+} alloying in concentrations up to $x = 1$ increases the Ce^{3+} luminescence contribution (Figure 4b, curves 2) in comparison with the CL spectra of Gd free SCF samples (Figure 4a, curve 1). Meanwhile, the Gd^{3+} alloying in the concentration range above $x = 1.0$ in $Tb_{3-x}Gd_xAl_{5-y}Ga_yO_{12}:Ce$ (PbO) SCFs also results in the notable decrease of the Ce^{3+} emission contribution to the total spectrum of the SCF luminescence and respective increase of the Tb^{3+} luminescence contribution (Figure 4a, curves 3–5). This can be caused by variation of the efficiency of $Gd^{3+} \rightarrow Tb^{3+}$ and $Tb^{3+} \rightarrow Ce^{3+}$ energy transfer processes in $Tb_{3-x}Gd_xAl_{5-y}Ga_yO_{12}:Ce$ SCFs due to the change of the respective positions of Ce^{3+} and Tb^{3+} absorption and emission bands at different concentration of Tb^{3+} and Gd^{3+} cations.

Based on the results presented in Figure 4a,b, we can confirm here that the optimal values of the Gd^{3+} and Ga^{3+} concentrations in $Tb_{3-x}Gd_xAl_{5-y}Ga_yO_{12}:Ce$ SCFs are $x = 1-1.5$ and $y = 2-2.5$ ranges, respectively. At these concentrations the respective CL spectra of $Tb_{1.5}Gd_{1.5}Al_{3-2.5}Ga_{2-2.5}O_{12}:Ce$ (PbO) and (BaO) SCFs show the dominant Ce^{3+} emission band with relatively small contribution of the Tb^{3+} luminescence (Figure 4b, curves 2 and 3 and Figure 4c, curves 1 and 2).

3.2. Scintillation Decay Kinetics

The scintillation decay kinetics of $Tb_{3-x}Gd_xAl_{5-y}Ga_yO_{12}:Ce$ and $Tb_{1.5}Gd_{1.5}Al_{5-y}Ga_yO_{12}:Ce$ SCFs, grown both from PbO (a) and BaO (b) fluxes with different x and y values in the 0–2 and 2–2.5 ranges, respectively, are shown correspondingly in Figure 5a,b. Generally, the $Tb_{3-x}Gd_xAl_{5-y}Ga_yO_{12}:Ce$ SCF scintillators demonstrate the notably slower non-exponential kinetics similarly to their YAG:Ce and LuAG:Ce SCF counterparts [21,36]. Such slower decay kinetics of the Ce^{3+} luminescence is typical for Tb^{3+} and Gd^{3+} based SCF scintillators, where the cascade energy transfer via both sublattices of Gd^{3+} and Tb^{3+} cations is more complicated [36] in comparison with their YAG:Ce and LuAG:Ce SCF analogues, where the direct energy transfer from the garnet host to Ce^{3+} ions dominates [21].

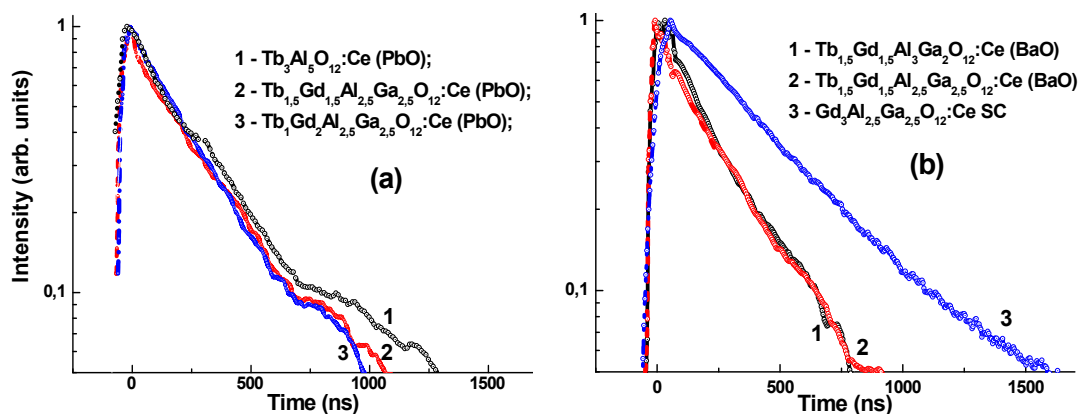


Figure 5. (a) The normalized scintillation decay kinetics of $Tb_{3-x}Gd_xAl_{2.5}Ga_{2.5}O_{12}:Ce$ (PbO) SCFs (curves 2, 3) with different Gd and Ga contents in comparison with the decay kinetics of the $Tb_3Al_5O_{12}:Ce$ (PbO) SCF counterpart (curve 1); (b) the normalized scintillation decay kinetics of $Tb_{1.5}Gd_{1.5}Al_{5-y}Ga_yO_{12}:Ce$ (BaO) SCFs (curves 1, 2) with different Ga content in comparison with the decay kinetics of $Gd_3Al_{2.5}Ga_{2.5}O_{12}:Ce$ bulk SC (curve 3).

The influence of Ga^{3+} and Gd^{3+} alloying on the scintillation decay of $Tb_{3-x}Gd_xAl_{5-y}Ga_yO_{12}:Ce$ (PbO) SCFs was firstly considered in [36]. We will explain the choice of optimal Gd^{3+} and Ga^{3+} concentrations in these SCFs in more detail based on the results of their scintillation decay kinetics (Figure 5a). The Ga^{3+} alloying with the concentration up to $y = 2.5$ in $Tb_3Al_{5-y}Ga_yO_{12}:Ce$ (PbO) SCFs leads to a significant slowdown of the decay kinetics of the Ce^{3+} emission in comparison with the TbAG:Ce SCF due to the lowering of the bottom of the conductive band and the arising electron

transitions from the excited levels of Ce^{3+} to the conductive band. This results in the strong elongation of the scintillation decay of $\text{Tb}_3\text{Al}_{5-y}\text{Ga}_y\text{O}_{12}:\text{Ce}$ (PbO) SCFs (not present in Figure 5a). Contrary to the influence of Ga^{3+} cations, the Gd^{3+} alloying in the concentration range $x = 1.5\text{--}2$ strongly accelerates the scintillation decay of $\text{Tb}_{3-x}\text{Gd}_x\text{Al}_{2.5}\text{Ga}_{2.5}\text{O}_{12}:\text{Ce}$ (PbO) SCFs (Figure 5a, curves 2 and 3). It is also important to note here that the scintillation decay times $t_{1/e}$ and $t_{1/20}$ in $\text{Tb}_{3-x}\text{Gd}_x\text{Al}_{5-y}\text{Ga}_y\text{O}_{12}$ (PbO) SCFs at high Gd and Ga concentrations ($x = 1.5\text{--}2$; $y = 2.5$) (Figure 5a, curves 2 and 3) are close or even faster with respect to the corresponding values for $\text{Tb}_3\text{Al}_5\text{O}_{12}:\text{Ce}$ SCF (see also Table 1).

The $\text{Tb}_{1.5}\text{Gd}_{1.5}\text{Al}_{5-y}\text{Ga}_y\text{O}_{12}:\text{Ce}$ SCF scintillators, grown from the BaO based flux (Figure 5b), demonstrate significantly more exponential kinetics than that in their SCF counterparts, grown from the PbO based flux (Figure 5a). Such a difference can be caused by eliminating the delay of energy transfer from the garnet hosts to Ce^{3+} ions caused by the defect centers related to the Pb^{2+} ions in $\text{Tb}_{3-x}\text{Gd}_x\text{Al}_{5-y}\text{Ga}_y\text{O}_{12}:\text{Ce}$ (PbO) SCF scintillators. The concentration of these defect centers is significantly smaller in their analogues, prepared from the BaO based flux due to the very low contamination with Ba^{2+} ions.

It is necessary also to note here that the scintillation decay of $\text{Tb}_{1.5}\text{Gd}_{1.5}\text{Al}_{3-2.5}\text{Ga}_{2-2.5}\text{O}_{12}:\text{Ce}$ (BaO) SCFs (Figure 5b, curves 1 and 2) is also notably faster than that in $\text{Gd}_3\text{Al}_{2.5}\text{Ga}_{2.5}\text{O}_{12}:\text{Ce}$ SC counterparts (Figure 5b, curve 3) which can also be used as a substrate for producing SCF scintillators. In such a way these SCFs and the high-quality $\text{Gd}_3\text{Al}_{2.5}\text{Ga}_{2.5}\text{O}_{12}:\text{Ce}$ SCs can also be used for the creation of advanced hybrid film-substrate scintillators using the LPE method for simultaneous registration of the different components of ionization fluxes [52]. In such scintillators, the separation of the signal coming from the film and crystal parts of the hybrid scintillator can be performed using the differences in their scintillation decay kinetics (Figure 5b, curves 1 and 3, respectively).

3.3. TSL Properties

The results of the TSL investigations after irradiation by alpha particles of $\text{Tb}_{3-x}\text{Gd}_x\text{Al}_{5-y}\text{Ga}_y\text{O}_{12}:\text{Ce}$ SCFs with different x and y values, grown from both PbO (a) and BaO (b) based fluxes, in the above RT range are shown in Figure 6. The TSL in these SCFs arises at the thermal liberation of electrons from traps and their recombination with the holes localized around Ce^{3+} ions [21,28,33,42,43]. Taking into account the low temperature of SCF preparation in oxygen containing atmosphere (air), the formation of these traps can be caused mainly by the presence of Pb^{2+} and Ba^{2+} (from flux) and Pt^{4+} (from crucible) contaminations in SCF samples. This leads to the creation of different locally non-compensated lattice defects, such as the oxygen or cation vacancies, around the mentioned impurities, which act as trapping centers [21,31,36,53,54].

In $\text{Tb}_3\text{Al}_5\text{O}_{12}:\text{Ce}$ (PbO) SCFs, the position of the main TSL peak is located at 440 K (Figure 6a, curve 1). Ga^{3+} alloying of $\text{Tb}_3\text{Al}_{5-x}\text{Ga}_x\text{O}_{12}:\text{Ce}$ SCFs in the concentration range up to $y = 2$ leads to the shift of the TSL peaks to 407 K and substantially decreases the TSL signal in the 350–600 K range (Figure 6a, curve 2) (see also [31,36]). Gd^{3+} alloying additionally shifts the TSL peak to 390 K and slightly decreases the TSL signal of $\text{Tb}_{1.5}\text{Gd}_{1.3}\text{Al}_{2.5}\text{Ga}_{2.5}\text{O}_{12}:\text{Ce}$ (PbO) SCFs in the 450–650 K high-temperature range in comparison with Gd free SCF samples (Figure 6a, curve 3). These results are in good correlation with the significant increase of the LY in $\text{Tb}_{1.5}\text{Gd}_{1.5}\text{Al}_{3-2.5}\text{Ga}_{2-2.5}\text{O}_{12}:\text{Ce}$ (PbO) SCFs (Table 1), most probably due to elimination of the participation of high-temperature trap-related centers in the scintillation processes in the SCF samples with the mentioned optimal content.

Using the lead free BaO based flux for the growth of $\text{Tb}_{3-x}\text{Gd}_x\text{Al}_{5-y}\text{Ga}_y\text{O}_{12}:\text{Ce}$ SCFs leads also to the low intensity of the TSL peaks in the above RT range in SCF scintillators (Figure 6b). Namely, the TSL intensity of $\text{Tb}_{1.5}\text{Gd}_{1.5}\text{Al}_{3-2.5}\text{Ga}_{2-2.5}\text{O}_{12}:\text{Ce}$ (BaO) SCFs in the 450–600 K range is also negligible (Figure 6b). This result is in good correlation with the high LY in $\text{Tb}_{1.5}\text{Gd}_{1.5}\text{Al}_{3-2.5}\text{Ga}_{2-2.5}\text{O}_{12}:\text{Ce}$ (BaO) SCFs (Table 1), due to the low Ba^{2+} contamination and related with them trapping centers as well as to the additional elimination of the trap-related phenomena in the scintillation processes in these SCFs by Ga^{3+} and Gd^{3+} alloying.

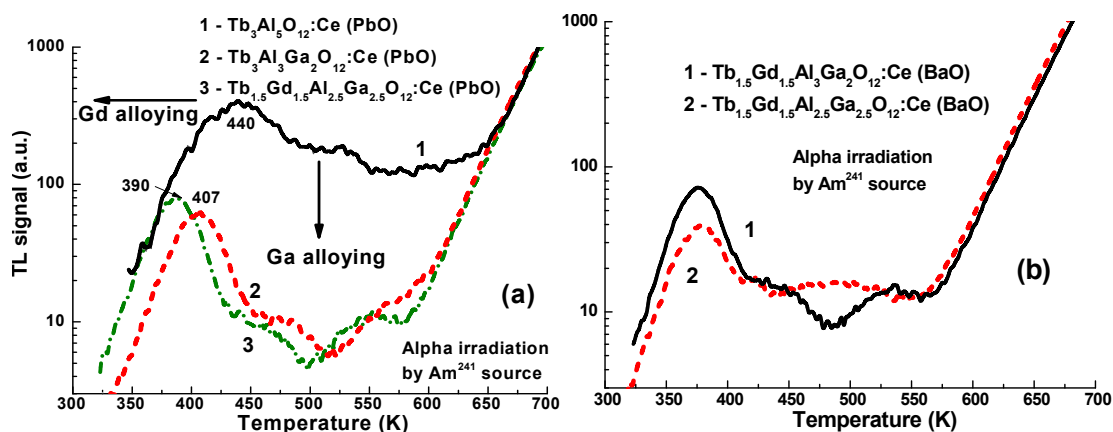


Figure 6. TSL (in the log scale) of $Tb_{3-x}Gd_xAl_{5-y}Ga_yO_{12}:Ce$ (PbO) (a) with a different content of Gd^{3+} and Ga^{3+} cations (see legend of the figure) and $Tb_{1.5}Gd_{1.5}Al_{3-2.5}Ga_{2-2.5}O_{12}:Ce$ (BaO) (b) SCFs after irradiation by Am^{241} α -particles and registration of the Ce^{3+} luminescence.

Thus, the Ga^{3+} alloying in the concentration range $y = 2-2.5$ positively affects not only the scintillation properties of melt-grown mixed garnet crystals with a large concentration of antisite defects and oxygen vacancies [22–24] but antisite free SCF counterparts as well [31–33] due to burying the trap levels by the bottom of the conductive band in the Ga-containing garnets. The additional positive effect on the elimination of the trap centers in scintillation phenomena, which is observed in $Tb_{3-x}Gd_xAl_{5-y}Ga_yO_{12}:Ce$ SCF samples, is most probably caused by burying the deeper trap levels by high-energy states of Tb^{3+} and Gd^{3+} cations in such Tb,Gd-rich garnets [36].

3.4. Photoelectron Light Yield Measurements

The scintillation LY of $Tb_{3-x}Gd_xAl_{5-y}Ga_yO_{12}:Ce$ SCFs, grown from PbO and BaO based fluxes at different content of Gd^{3+} and Ga^{3+} cations, measured with a shaping time of 14 μs under excitation by α -particles of Pu^{239} (5.15 MeV) source, is shown in Table 1 and Figure 7.

In principle, the simultaneous influence of Gd^{3+} and Ga^{3+} doping of TbAG:Ce SCFs can also result in a strong increase in the LY of $Tb_{3-x}Gd_xAl_{5-y}Ga_yO_{12}:Ce$ SCF scintillators at $x = 0-1.5$ and $y = 2-3$ [21,36]. Thus, the determination of the optimal content and ratio between the Gd^{3+} and Ga^{3+} cations in the TbAG:Ce garnet host is the most important task for the optimization of the properties of $Tb_{3-x}Gd_xAl_{5-y}Ga_yO_{12}:Ce$ SCF scintillators in the case of growth from both PbO and especially lead free BaO based flux.

We have observed that Ga^{3+} doping in the concentration range $y = 2-2.5$ leads to the increase of the LY of $Tb_3Al_{5-y}Ga_yO_{12}:Ce$ (PbO) SCF scintillators. Indeed, with the Ga^{3+} doping at the concentration $y = 2.5$, the LY of these scintillators notably (up to 20%) overcomes the LY of the $Tb_3Al_5O_{12}:Ce$ SCF sample (Table 1). This is caused mainly by the elimination of trap-related phenomena in $Tb_3Al_{5-y}Ga_yO_{12}:Ce$ SCF scintillators due to the decrease of the $Tb_3Al_5O_{12}$ band gap in the case of Ga alloying in the mentioned concentration range (see Part 3.3 for details).

In addition to the positive trend caused by the doping with Ga^{3+} ions, the significant increase of the LY is observed in $Tb_{3-x}Gd_xAl_{5-y}Ga_yO_{12}:Ce$ (PbO) SCFs due to Gd^{3+} doping at the concentration $x = 1-1.5$ (Table 1). This effect can be caused by the deepest localization of the Ce^{3+} emitting levels inside the band gap and better separation of them with respect to the levels of conductive band. Namely, the $Tb_{1.5}Gd_{1.5}Al_{2.5}Ga_{2.5}O_{12}:Ce$ (PbO) SCF possess excellent scintillation properties (Table 1 and Figure 7). The photoelectron LY of this SCF sample significantly overcomes the LY of the best samples of LuAG:Ce SCF [53], $Lu_{1.5}Gd_{1.5}Al_{2.75}Ga_{2.25}O_{12}:Ce$ SCF [31] and $Tb_3Al_5O_{12}:Ce$ SCF [21], grown from PbO based flux, up to 1.85, 2.62 and 1.95 times, respectively (see Table 1). This LY is

the highest one ever obtained in our group for the garnet SCF scintillators grown by the LPE from traditional PbO-B₂O₃ based flux [21,31,36,38,53].

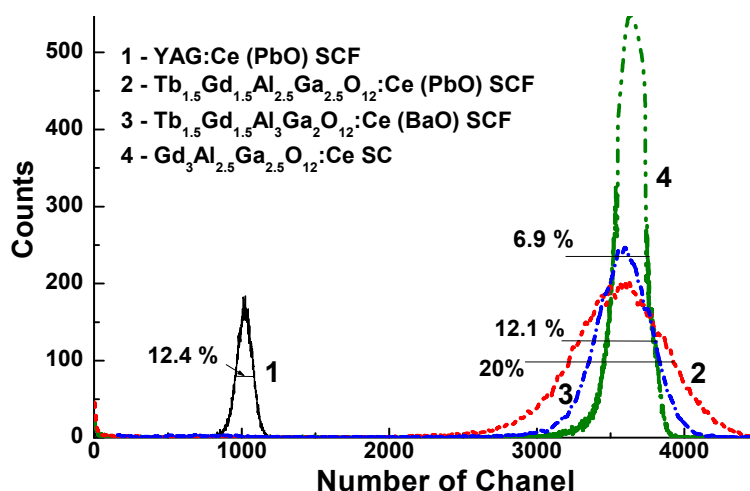


Figure 7. Pulse height spectra of Tb_{1.5}Gd_{1.5}Al_{2.5}Ga_{2.5}O₁₂:Ce (PbO) (2) (LY = 1368 phels/MeV (380%); E = 20%) and Tb_{1.5}Gd_{1.5}Al₃Ga₂O₁₂:Ce (BaO) (3) (LY = 1370 phels/MeV (380%); E = 12.1%) in comparison with YAG:Ce SCFs (1) (LY = 360 phels/MeV (100%), E = 12.4%) and Gd₃Al_{2.5}Ga_{2.5}O₁₂:Ce SC (4) (LY = 1375 phels/MeV (381%); E = 6.9%) excited by α -particles of ²³⁹Pu (5.15 MeV) source and registered with a shaping time of 14 μ s.

The elimination of Pb²⁺ contamination by using the lead-free BaO based flux in principle can result in the improvement of the LY and energy resolution of Tb_{3-x}Gd_xAl_{5-y}Ga_yO₁₂:Ce SCF scintillators (Table 1 and Figure 7). Indeed, the Tb_{1.5}Gd_{1.5}Al₃Ga₂O₁₂:Ce (BaO) SCF sample also possess excellent scintillation properties. Probably due to the elimination of the quenching and trap related phenomena caused by lead ions, the best LY and energy resolution in these SCF is observed at lower Ga concentration y = 2 in the Tb_{1.5}Gd_{1.5}Al₃Ga₂O₁₂:Ce (BaO) SCF sample than in the case of using the PbO based flux (Table 1). The LY of these SCFs also notably (up to 10%) exceeds the LY of the best Lu_{3-x}Gd_xAl_{5-y}Ga_yO₁₂:Ce (BaO) and Gd₃Al_{5-y}Ga_xO₁₂:Ce (BaO) SCF scintillators [31] (Table 1). *Without doubt, this is the highest LY for garnet SCF scintillators, grown by the LPE method from BaO based flux in our group [31].* However, the increase of the LY of Tb_{3-x}Gd_xAl_{5-y}Ga_yO₁₂:Ce SCFs due to the elimination of negative influence of Pb²⁺ flux related dopants is relatively small and is not so significant as in the case of producing Lu_{1-x}Gd_xAl_{5-y}Ga_yO₁₂:Ce and Gd₃Al_{5-y}Ga_yO₁₂:Ce SCFs scintillators from PbO and BaO based fluxes [31]. This can be caused by a more favourable situation in terms of the energy transfer phenomena via the sublattice of Tb³⁺ cations to Ce³⁺ ions in the case of Tb_{3-x}Gd_xAl_{5-y}Ga_yO₁₂:Ce (PbO) SCFs which enables the production of these scintillators with high LY and excellent structural quality from the traditional PbO based flux.

Thus, the main reason for such an increase of the LY of Tb_{3-x}Gd_xAl_{5-y}Ga_yO₁₂:Ce SCFs is the optimized cation content with respect to the crystal field strength and energy transfer efficiency to Ce³⁺ ions directly from the mixed garnet host and via the sublattice of Tb³⁺ and Gd³⁺ cations. Most probably, the relative position of Ce³⁺ levels with respect to the levels of Tb³⁺ and Gd³⁺ cations is optimal in Tb_{1.4-1.5}Gd_{1.6-1.5}Al_{3-2.5}Ga_{2-2.5}O₁₂:Ce garnet hosts from the point of view of efficiency of the complicated Gd³⁺ → Tb³⁺ → Ce³⁺ → Tb³⁺ energy transfer in these matrixes. The details of such a transfer are presented in the separate papers [34,35,49–51].

It is also important to note that the LY of Tb_{1.5}Gd_{1.5}Al_{2.5}Ga_{2.5}O₁₂:Ce (PbO) and Tb_{1.5}Gd_{1.5}Al₃Ga₂O₁₂:Ce (BaO) SCFs is comparable with that in the high-quality Gd₃Al_{2.5-2}Ga_{2.5-3}O₁₂:Ce SC samples (Table 1 and Figure 7). This also enables producing the hybrid film-substrate detectors using the LPE method with high LY both in film and substrate scintillators with optimized contents, taking into

account the requirement for the decay times of the signals coming from the film and substrate components of the hybrid scintillator differs by a factor of at least two [52]. Such a demand is fully realized in the case of $\text{Tb}_{1.5}\text{Gd}_{1.5}\text{Al}_3\text{Ga}_2\text{O}_{12}:\text{Ce}$ (BaO) SCF/ $\text{Gd}_3\text{Al}_{2.5}\text{Ga}_{2.5}\text{O}_{12}:\text{Ce}$ SC hybrid scintillators (Figure 4b). These scintillators can be proposed for different types of application, especially for registration of the components of mixed ionizing flux [52] and multi-layer screens for visualization of X-ray images [21].

4. Conclusions

In this work, we report the creation of advanced single crystalline film (SCF) screens with excellent scintillation properties based on the $\text{Tb}_{1.5}\text{Gd}_{1.5}\text{Al}_{3-2.5}\text{Ga}_{2-2.5}\text{O}_{12}:\text{Ce}$ mixed garnet compounds grown by the LPE method from both novel lead free BaO and traditional PbO based fluxes onto $\text{Gd}_3\text{Al}_{2.5}\text{Ga}_{2.5}\text{O}_{12}$ (GAGG) substrates.

The optimization of Gd^{3+} and Ga^{3+} content in the $\text{Tb}_{3-x}\text{Gd}_x\text{Al}_{5-y}\text{Ga}_y\text{O}_{12}:\text{Ce}$ garnet at $x = 1.5$ and $y = 2-2.5$ results in the strong improvement of the energy transfer efficiency from the $\text{Tb}^{3+}\text{-Gd}^{3+}$ based matrix to Ce^{3+} ions due to the modification of the band gap value and Ce^{3+} energy structure, as well as the elimination of the TSL peaks above room temperature. Namely, the $\text{Tb}_{1.5}\text{Gd}_{1.5}\text{Al}_3\text{Ga}_2\text{O}_{12}:\text{Ce}$ SCFs grown from BaO based flux under α -particle excitation possess the highest LY values among all the LPE grown garnet SCF scintillators obtained in our group, which exceeds by at least 10% the LY of the best samples of the recently developed $\text{Lu}_{1.5}\text{Gd}_{1.5}\text{Al}_{2.75}\text{Ga}_{2.25}\text{O}_{12}:\text{Ce}$ and $\text{Gd}_3\text{Al}_{2.75}\text{Ga}_{2.25}\text{O}_{12}:\text{Ce}$ SCF scintillators grown from BaO based flux [31]. The photoelectron LY of these SCF scintillators under excitation by ^{239}Pu (5.15 MeV) source is comparable with that in high-quality $\text{Gd}_3\text{Al}_{2.5-3}\text{Ga}_{2.5-3}\text{O}_{12}:\text{Ce}$ reference bulk crystal analogue with a photoelectron LY of 1370 phels/MeV (light yield of about 10,000 photons/MeV). $\text{Tb}_{1.5}\text{Gd}_{1.5}\text{Al}_3\text{Ga}_2\text{O}_{12}:\text{Ce}$ SCFs also have a relatively fast scintillation response in the hundred ns range under α -particle excitation with decay times $t_{1/e}$ and $t_{1/20}$ of 230 and 730 ns, respectively. Meanwhile, the structural uniformity and optical quality of these SCF scintillators are strongly influenced by the high-viscosity of BaO based melt.

The SCFs of $\text{Tb}_{1.5}\text{Gd}_{1.5}\text{Al}_{2.5}\text{Ga}_{2.5}\text{O}_{12}:\text{Ce}$ garnets, grown from PbO based flux onto GAGG substrates, possess very high structural quality and excellent scintillation properties. Under α -particle excitation, the LY of $\text{Tb}_{1.5}\text{Gd}_{1.5}\text{Al}_{2.5}\text{Ga}_{2.5}\text{O}_{12}:\text{Ce}$ (PbO) SCFs is comparable with that of their analogues grown from BaO flux and these SCFs possess only slightly slower scintillation response with decay times $t_{1/e}$ and $t_{1/20}$ of 330 and 990 ns, respectively. It is important to note that the negative quenching influence of the Pb^{2+} flux related dopants is not so significant during manufacturing the $\text{Tb}_{1.5}\text{Gd}_{1.5}\text{Al}_{2.5}\text{Ga}_{2.5}\text{O}_{12}:\text{Ce}$ SCF scintillators as in the case of $\text{Lu}_{1-x}\text{Gd}_x\text{Al}_{5-y}\text{Ga}_y\text{O}_{12}:\text{Ce}$ and $\text{Gd}_3\text{Al}_{5-y}\text{Ga}_y\text{O}_{12}:\text{Ce}$ SCFs analogues grown from PbO based fluxes [31]. This enables the production of $\text{Tb}_{3-x}\text{Gd}_x\text{Al}_{5-y}\text{Ga}_y\text{O}_{12}:\text{Ce}$ SCF scintillators with high LY and excellent structural quality from the traditional PbO based flux. Most probably, this positive trend is observed only in the Tb containing scintillators, where very complicated but efficient energy transfer from Tb^{3+} and Gd^{3+} cation sub-lattices to Ce^{3+} ions can be realized in comparison with Lu- and Gd-containing scintillators where such transfer is absent.

We have also found that the scintillation decay of $\text{Tb}_{1.5}\text{Gd}_{1.5}\text{Al}_{2.5}\text{Ga}_{2.5}\text{O}_{12}:\text{Ce}$ (PbO) and especially $\text{Tb}_{1.5}\text{Gd}_{1.5}\text{Al}_3\text{Ga}_2\text{O}_{12}:\text{Ce}$ (BaO) SCFs in the 0–2 μs range is notably faster (at least by 2 times) than that in $\text{Gd}_3\text{Al}_{2.5}\text{Ga}_{2.5}\text{O}_{12}:\text{Ce}$ SC counterparts which can also be used as a substrate for producing SCF scintillators. In such a way these SCFs and the high-quality $\text{Gd}_3\text{Al}_{2.5}\text{Ga}_{2.5}\text{O}_{12}:\text{Ce}$ crystals can be used for the creation of hybrid film-substrate scintillators using the LPE method for simultaneous registration of the different components of ionization fluxes. In such types of hybrid scintillators, the separation of the signal coming from the film and crystal parts can be performed using the differences in the scintillation decay kinetics.

Acknowledgments: The work was performed in the framework of NCN No 2016/21/B/ST8/03200 and NCBR NANOLUX2014 No 286 projects and also partly supported by the Ministry of Education and Science of Ukraine in the framework of SF-20 F projects.

Author Contributions: Vitalii Gorbenko performed the SCF growth experiments and wrote growth part of paper, Tetiana Zorenko performed the scintillation LY and decay kinetic measurements, Kazimierz Paprocki performed the CL spectra measurements; Alexander Fedorov performed the XRD investigations and analysis of SCF structural quality, Oleg Sidletskiy performed the GAGG substrates preparation; Sandra Witkiewicz collected and analyzed the SCF optical properties; Paweł Bilski and Anna Twardak performed the TSL measurements of the SCF samples and Yuriy Zorenko analyzed experimental materials and wrote the Introduction, Third part and Conclusion of the paper.

Conflicts of Interest: The authors declare no conflict of interest.

References

1. Koch, A.; Raven, C.; Spanne, P.; Snigirev, A. X-ray imaging with submicrometer resolution employing transparent luminescent screens. *J. Opt. Soc. Am. A* **1998**, *15*, 1940–1951. [[CrossRef](#)]
2. Koch, A.; Peyrin, F.; Heurtier, P.; Ferrand, B.; Chambaz, B.; Ludwig, W.; Couchaud, M. X-ray camera for computed microtomography of biological samples with micrometer resolution using $\text{Lu}_3\text{Al}_5\text{O}_{12}$ and $\text{Y}_3\text{Al}_5\text{O}_{12}$ scintillators. *Proc. SPIE* **1999**, *3659*, 170–179.
3. Martin, T.; Koch, A. Recent developments in X-ray imaging with micrometer spatial resolution. *J. Synchrotron Radiat.* **2006**, *13*, 180–194. [[CrossRef](#)] [[PubMed](#)]
4. Zorenko, Y.; Gorbenko, V.; Voznyak, T.; Martin, T.; Douissard, P.-A.; Mares, J.A.; Nikl, M. LuAG:Pr, LuAG:La, and LuAP:Ce thin film scintillators for visualisation of X-ray images. *Int. Soc. Opt. Photonics* **2009**, *7310*, 731007.
5. Martin, T.; Douissard, P.-A.; Couchaud, M.; Cecilia, A.; Baumbach, T.; Dupré, K.; Rack, A. LSO-based single crystal film scintillator for synchrotron-based hard X-ray micro-imaging. *IEEE Trans. Nucl. Sci.* **2009**, *56*, 1412–1418. [[CrossRef](#)]
6. Douissard, P.-A.; Cecilia, A.; Rochet, X.; Chapel, X.; Martin, T.; Van De Kamp, T.; Helfen, L.; Baumbach, T.; Luquot, L.; Xiao, X.; et al. A versatile indirect detector design for hard X-ray microimaging. *J. Instrum.* **2012**, *7*, P09016. [[CrossRef](#)]
7. Douissard, P.-A.; Cecilia, A.; Martin, T.; Chevalier, V.; Couchaud, M.; Baumbach, T.; Dupré, K.; Kühbacher, M.; Rack, A. A novel epitaxially grown LSO-based thin-film scintillator for micro-imaging using hard synchrotron radiation. *J. Synchrotron Radiat.* **2010**, *17*, 571–583. [[CrossRef](#)] [[PubMed](#)]
8. Cecilia, A.; Rack, A.; Douissard, P.-A.; Martin, T.; dos Santos Rolo, T.; Vagovič, P.; Hamann, E.; van de Kamp, T.; Riedel, A.; Fiederle, M.; et al. LPE grown LSO:Tb scintillator films for high-resolution X-ray imaging applications at synchrotron light sources. *Nucl. Instrum. Meth. A* **2011**, *648*, S321–S323. [[CrossRef](#)]
9. Zorenko, Y.; Nikl, M.; Gorbenko, V.; Savchyn, V.; Voznyak, T.; Kucerkova, R.; Sidletskiy, O.; Grinyov, B.; Fedorov, A. Growth and luminescent properties of Lu_2SiO_5 and $\text{Lu}_2\text{SiO}_5:\text{Ce}$ single crystalline films. *Opt. Mater.* **2011**, *33*, 846–852. [[CrossRef](#)]
10. Zorenko, Y.; Gorbenko, V.; Savchyn, V.; Voznyak, T.; Grinyov, B.; Sidletskiy, O.; Kurtsev, D.; Fedorov, A.; Baumer, V.; Nikl, M.; et al. Growth and luminescent properties of $\text{Lu}_2\text{SiO}_5:\text{Ce}$ and $(\text{Lu}_{1-x}\text{Gd}_x)_2\text{SiO}_5:\text{Ce}$ single crystalline films. *J. Cryst. Growth* **2011**, *337*, 72–80. [[CrossRef](#)]
11. Zorenko, Y.; Gorbenko, V.; Savchyn, V.; Voznyak, T.; Gorbenko, V.V.; Nikl, M.; Mares, J.A.; Sidletskiy, O.; Grinyov, B.; Fedorov, A.; et al. Scintillation and luminescent properties of undoped and Ce^{3+} doped Y_2SiO_5 and Lu_2SiO_5 single crystalline films grown by LPE method. *Opt. Mater.* **2012**, *34*, 1969–1974. [[CrossRef](#)]
12. Zorenko, Y.; Gorbenko, V.; Savchyn, V.; Zorenko, T.; Grinyov, B.; Sidletskiy, O.; Fedorov, A.; Mares, J.A.; Nikl, M.; Kucera, M. $\text{Lu}_2\text{SiO}_5:\text{Ce}$ and $\text{Y}_2\text{SiO}_5:\text{Ce}$ single crystals and single crystalline film scintillators: Comparison of the luminescent and scintillation properties. *Radiat. Meas.* **2013**, *56*, 84–89. [[CrossRef](#)]
13. Twardak, A.; Bilski, B.; Zorenko, Y.; Zorenko, T.; Gorbenko, V.; Mandowska, E.; Mandowski, A.; Sidletskiy, O.; Mares, J. Thermoluminescent properties of undoped and Ce-Doped lutetium orthosilicate and yttrium orthosilicate single crystals and single crystalline films scintillators. *IEEE Trans. Nucl. Sci.* **2014**, *61*, 276–281. [[CrossRef](#)]
14. Zorenko, Y.; Gorbenko, V.; Savchyn, V.; Zorenko, T.; Grinyov, B.; Sidletskiy, O.; Fedorov, A. Growth and luminescent properties of Ce and Ce-Tb doped $(\text{Y, Lu, Gd})_2\text{SiO}_5:\text{Ce}$ single crystalline films. *J. Cryst. Growth* **2014**, *401*, 577–583. [[CrossRef](#)]
15. Riva, F. Towards a New Generation of Thin Scintillating Films to Fit the Synchrotron Needs. Available online: <http://www.success.kharkov.ua/news/4ws/riva.pdf> (accessed on 27 August 2017).

16. Zorenko, Y.; Gorbenko, V.; Nikl, M.; Mares, J.A.; Martin, T.; Douissard, P.-A. Development of novel UV emitting single crystalline film scintillators. *IEEE Trans. Nucl. Sci.* **2010**, *57*, 1335–1342. [[CrossRef](#)]
17. Zorenko, Y.; Gorbenko, V.; Savchyn, V.; Voznyak, T.; Sidletskiy, O.; Grinyov, B.; Nikl, M.; Mares, J.A.; Martin, T.; Douissard, P.-A. Single crystalline film scintillators based on the orthosilicate, perovskite and garnet compounds. *IEEE Trans. Nucl. Sci.* **2012**, *59*, 2260–2268. [[CrossRef](#)]
18. Douissard, P.-A.; Martin, T.; Riva, F.; Mathieu, E.; Zorenko, Y.; Savchyn, V.; Zorenko, T.; Fedorov, A. Scintillating screens for micro-imaging based on the Ce-Tb doped LuAP single crystal films. *IEEE Trans. Nucl. Sci.* **2014**, *61*, 433–438. [[CrossRef](#)]
19. Riva, F.; Douissard, P.-A.; Martin, T.; Carlá, F.; Zorenko, Y.; Dujardin, C. Epitaxial growth of gadolinium and lutetium-based aluminum perovskite thin films for X-ray micro-imaging applications. *CrystEngComm* **2016**, *18*, 608–615. [[CrossRef](#)]
20. Zorenko, Y.; Gorbenko, V. Growth peculiarities of the $R_3Al_5O_{12}$ ($R = Lu, Yb, Tb, Eu-Y$) single crystalline film phosphors by liquid phase epitaxy. *Radiat. Meas.* **2007**, *42*, 907–910. [[CrossRef](#)]
21. Zorenko, Y.; Douissard, P.-A.; Martin, T.; Riva, F.; Gorbenko, V.; Zorenko, T.; Paprocki, K.; Iskaliyeva, A.; Witkiewicz, S.; Fedorov, A. Scintillating screens based on the LPE grown $Tb_3Al_5O_{12}:Ce$ single crystalline films. *Opt. Mater.* **2017**, *65*, 73–81. [[CrossRef](#)]
22. Kamada, K.; Endo, T.; Tsutumi, K.; Yanagida, T.; Fujimoto, Y.; Fukabori, A.; Yoshikawa, A.; Pejchal, J.; Nikl, M. Composition engineering in cerium-doped $(Lu, Gd)_3(Ga, Al)_5O_{12}$ single-crystal scintillators. *Cryst. Growth Des.* **2011**, *11*, 4484–4490. [[CrossRef](#)]
23. Kamada, K.; Kurosawa, S.; Prusa, P.; Nikl, M.; Kochurikhin, V.V.; Endo, T.; Tsutumi, K.; Sato, H.; Yokota, Y.; Sugiyama, K.; et al. Cz grown 2-in. size $Ce:Gd_3(Al, Ga)_5O_{12}$ single crystal; relationship between Al, Ga site occupancy and scintillation properties. *Opt. Mater.* **2014**, *36*, 1942–1945. [[CrossRef](#)]
24. Kamada, K.; Nikl, M.; Kurosawa, S.; Beitlerova, A.; Nagura, A.; Shoji, Y.; Pejchal, J.; Ohashi, Y.; Yokota, Y.; Yoshikawa, A. Alkali earth co-doping effects on luminescence and scintillation properties of Ce doped $Gd_3Al_2Ga_3O_{12}$ scintillator. *Opt. Mater.* **2015**, *41*, 63–66. [[CrossRef](#)]
25. Wang, C.; Wu, Y.; Ding, D.; Li, H.; Chen, X.; Shi, J.; Ren, G. Optical and scintillation properties of Ce-doped $(Gd_2Y_1)Ga_{2.7}Al_{2.3}O_{12}$ single crystal grown by Czochralski method. *Nucl. Instrum. Meth. A* **2016**, *820*, 8–13. [[CrossRef](#)]
26. Zorenko, Y.; Gorbenko, V.; Savchyn, V.; Zorenko, T.; Fedorov, A.; Wrzesiński, H.; Vasylykiv, Y. Multi-component Ce doped $(Gd, Y, La, Lu)_3(AlGaSc)_5O_{12}$ garnets—A new story in the development of scintillating single crystalline film screens. *Radiat. Meas.* **2013**, *56*, 150–154. [[CrossRef](#)]
27. Zorenko, Y.; Gorbenko, V.; Savchyn, V.; Zorenko, T.; Fedorov, A.; Sidletskiy, O. Novel scintillating screens based on the single crystalline films of Ce doped multi-component $(Gd, Y, Lu)_3(Al, Sc)_5O_{12}$ garnets. *IEEE Trans. Nucl. Sci.* **2014**, *61*, 439–442. [[CrossRef](#)]
28. Zorenko, Y.; Gorbenko, V.; Savchyn, V.; Zorenko, T.; Fedorov, A.; Sidletskiy, O. Development of scintillating screens based on the single crystalline films of Ce doped $(Gd, Y)_3(Al, Ga, Sc)_5O_{12}$ multi-component garnets. *J. Cryst. Growth* **2014**, *401*, 532–536. [[CrossRef](#)]
29. Zorenko, Y.; Gorbenko, V.; Vasylykiv, J.; Zelenyj, A.; Fedorov, A.; Kucerkova, R.; Mares, J.A.; Nikl, M.; Bilski, P.; Twardak, A. Growth and luminescent properties of scintillators based on the single crystalline films of $Lu_{3-x}Gd_xAl_5O_{12}:Ce$ garnet. *Mater. Res. Bull.* **2015**, *64*, 355–363. [[CrossRef](#)]
30. Zorenko, Y.; Gorbenko, V.; Vasylykiv, J.; Strzyżewski, T.; Fedorov, A.; Kucerkova, R.; Mares, J.A.; Nikl, M.; Bilski, P.; Twardak, A. Growth and luminescent properties of scintillators based on the single crystalline films of $(Lu, Gd)_3(Al, Ga)_5O_{12}:Ce$ garnets. *J. Lumin.* **2016**, *169*, 828–837. [[CrossRef](#)]
31. Zorenko, Y.; Gorbenko, V.; Zorenko, T.; Sidletskiy, O.; Fedorov, A.; Bilski, P.; Twardak, A. High-performance Ce-doped multicomponent garnet single crystalline film scintillators. *Phys. Status Solidi-R.* **2015**, *9*, 489–493. [[CrossRef](#)]
32. Prusa, P.; Kucera, M.; Mares, J.A.; Hanus, M.; Beitlerova, A.; Onderisínova, Z.; Nikl, M. Scintillation properties of the Ce-doped multicomponent garnet epitaxial films. *Opt. Mater.* **2013**, *35*, 2444–2448. [[CrossRef](#)]
33. Prusa, P.; Kucera, M.; Mares, J.A.; Onderisínova, Z.; Hanus, M.; Babin, V.; Beitlerova, A.; Nikl, M. Composition tailoring in Ce-doped multicomponent garnet epitaxial film scintillators. *Cryst. Growth Des.* **2015**, *15*, 3715–3723. [[CrossRef](#)]

34. Bartosiewicz, K.; Babin, V.; Nikl, M.; Mares, J.A.; Zorenko, Y.; Gorbenko, V. Luminescence and energy transfer processes in $(\text{Lu, Tb})_3\text{Al}_5\text{O}_{12}$ single crystalline films doped with Ce^{3+} . *J. Lumin.* **2016**, *173*, 141–148. [[CrossRef](#)]
35. Bartosiewicz, K.; Babin, V.; Mares, J.A.; Beitlerova, A.; Zorenko, Y.; Iskaliyeva, A.; Gorbenko, V.; Bryknar, Z.; Nikl, M. Luminescence and energy transfer processes in Ce^{3+} activated $(\text{Gd, Tb})_3\text{Al}_5\text{O}_{12}$ single crystalline films. *J. Lumin.* **2017**, *188*, 60–66. [[CrossRef](#)]
36. Zorenko, Y.; Gorbenko, V.; Zorenko, T.; Paprocki, K.; Bilski, P.; Twardak, A.; Voznyak, T.; Sidletskiy, O.; Gerasimov, Y.; Grynirov, B.; et al. Composition engineering of single crystalline films based on the multicomponent garnet compounds. *Opt. Mater.* **2016**, *61*, 3–10. [[CrossRef](#)]
37. Zorenko, Y.; Nikl, M.; Mares, J.A.; Gorbenko, V.; Savchyn, V.; Voznyak, T.; Kucera, M.; Beitlerova, A.; Kucerkova, R.; Fedorov, A. The luminescent and scintillation properties of YAlO_3 and $\text{YAlO}_3:\text{Ce}$ single crystalline films grown by liquid phase epitaxy from BaO-based flux. *Phys. Status Solidi A* **2009**, *206*, 2586–2592. [[CrossRef](#)]
38. Mares, J.A.; Beitlerova, A.; Nikl, M.; Solovieva, N.; Nitsch, K.; Kucera, M.; Kubova, M.; Gorbenko, V.; Zorenko, Y. Scintillation and optical properties of YAG:Ce films grown by liquid phase epitaxy. *Radiat. Meas.* **2007**, *42*, 533–536. [[CrossRef](#)]
39. Chani, V.I.; Yoshikawa, A.; Machida, H.; Fukuda, T. $(\text{Tb, Yb})_3\text{Al}_5\text{O}_{12}$ garnet: Crystal-chemistry and fiber growth by micro-pulling-down technique. *Mat. Sci. Eng. B* **2000**, *75*, 53–60. [[CrossRef](#)]
40. Fasoli, M.; Vedda, A.; Nikl, M.; Jiang, C.; Uberuaga, B.; Andersson, D.; McClellan, K.; Stanek, C.R. Band-gap engineering for removing shallow traps in rare-earth $\text{Lu}_3\text{Al}_5\text{O}_{12}$ garnet scintillators using Ga^{3+} doping. *Phys. Rev. B* **2011**, *84*, 081102. [[CrossRef](#)]
41. Geller, S.; Espinosa, G.P.; Fullmer, L.D.; Crandall, P.B. Thermal expansion of some garnets. *Mater. Res. Bull.* **1972**, *7*, 1219–1224. [[CrossRef](#)]
42. Ashurov, M.K.; Voronko, Y.; Osiko, V.V.; Sobol, A.A.; Timoshechkin, M.I. Spectroscopic study of stoichiometry deviation in crystals with garnet structure. *Phys. Status Solidi A* **1977**, *42*, 101–110. [[CrossRef](#)]
43. Lupei, V.; Lupei, A.; Tiseanu, C.; Georgescu, S.; Stoicescu, C.; Nanau, P.M. High-resolution optical spectroscopy of YAG:Nd: A test for structural and distribution models. *Phys. Rev. B* **1995**, *51*, 8–17. [[CrossRef](#)]
44. Kuklja, M.M. Defects in yttrium aluminium perovskite and garnet crystals: Atomistic study. *J. Phys. Condens. Mater.* **2000**, *12*, 2953–2967. [[CrossRef](#)]
45. Zorenko, Y.; Voloshinovskii, A.; Savchyn, V.; Voznyak, T.; Nikl, M.; Nejezchleb, K.; Mikhailin, V.; Kolobanov, V.; Spassky, D. Exciton and antisite defect-related luminescence in $\text{Lu}_3\text{Al}_5\text{O}_{12}$ and $\text{Y}_3\text{Al}_5\text{O}_{12}$ garnets. *Phys. Status Solidi B* **2007**, *244*, 2180–2189. [[CrossRef](#)]
46. Zorenko, Y.; Voloshynovskii, A.; Vistovsky, V.; Grinberg, M.; Kornlyo, A.; Łukasiewicz, T.; Świrkwicz, M. Antisite defect-related luminescence in $(\text{LaLu})_3\text{Lu}_2\text{Ga}_3\text{O}_{12}$ garnet single crystals. *Phys. Status Solidi B* **2007**, *244*, 3271–3278. [[CrossRef](#)]
47. Kummer, F.; Zwaschka, F.; Ellens, A.; Debray, A.; Waitl, G. Luminous Substance for a Light Source and Light Source Associated Therewith. U.S. Patent WO/2001/008452, 1 February 2001.
48. Batentschuk, M.; Osvet, A.; Schierning, G.; Klier, A.; Schneider, J.; Winnacker, A. Simultaneous excitation of Ce^{3+} and Eu^{3+} ions in $\text{Tb}_3\text{Al}_5\text{O}_{12}$. *Radiat. Meas.* **2004**, *38*, 539–543. [[CrossRef](#)]
49. Turos-Matysiak, R.; Gryk, W.; Grinberg, M.; Lin, Y.S.; Liu, R.S. $\text{Tb}^{3+} \rightarrow \text{Ce}^{3+}$ energy transfer in $\text{Y}_{3-x-y}\text{Tb}_y\text{Gd}_x\text{Al}_5\text{O}_{12}$ ($x = 0.65$, $y = 0.575$) doped with Ce^{3+} . *Radiat. Meas.* **2007**, *42*, 755–758. [[CrossRef](#)]
50. Zorenko, Y.; Voznyak, T.; Vistovsky, V.; Zorenko, T.; Nedilko, S.; Batentschuk, M.; Osvet, A.; Winnacker, A.; Zimmerer, G.; Kolobanov, V.; et al. Energy transfer to Ce^{3+} ions in $\text{Tb}_3\text{Al}_5\text{O}_{12}:\text{Ce}$ single crystalline films. *Radiat Meas.* **2007**, *42*, 648–651. [[CrossRef](#)]
51. Zorenko, Y.; Gorbenko, V.; Voznyak, T.; Zorenko, T.; Kuklinski, B.; Turos-Matysiak, R.; Grinberg, M. Luminescence properties of phosphors based on $\text{Tb}_3\text{Al}_5\text{O}_{12}$ (TbAG) terbium-aluminum garnet. *Opt. Spectrosc.* **2009**, *106*, 365–374. [[CrossRef](#)]
52. Zorenko, Y.V.; Novosad, S.S.; Pashkovskii, M.V.; Lyskovich, A.B.; Savitskii, V.G.; Batenchuk, M.M.; Malyutenkov, P.S.; Patsagan, N.I.; Nazar, I.V.; Gorbenko, V.I. Epitaxial structures of garnets as scintillation detectors of ionizing radiation. *J. Appl. Spectrosc.* **1990**, *52*, 645–649. [[CrossRef](#)]

53. Douissard, P.-A.; Martin, T.; Riva, F.; Zorenko, Y.; Zorenko, T.; Paprocki, K.; Bilski, P.; Twardak, A. Epitaxial growth of LuAG:Ce and LuAG:Ce, Pr films and their scintillation properties. *IEEE Trans. Nucl. Sci.* **2016**, *63*, 1726–1732. [[CrossRef](#)]
54. Nikl, M.; Mihokova, E.; Pejchal, J.; Vedda, A.; Zorenko, Y.; Nejezchleb, K. The antisite LuAl defect-related trap in Lu₃Al₅O₁₂:Ce single crystal. *Phys. Status Solidi B* **2005**, *242*, R119–R121. [[CrossRef](#)]



© 2017 by the authors. Licensee MDPI, Basel, Switzerland. This article is an open access article distributed under the terms and conditions of the Creative Commons Attribution (CC BY) license (<http://creativecommons.org/licenses/by/4.0/>).